# Electronic Excitations in the Edge-shared Relativistic Mott Insulator: $Na_2IrO_3$

Beom Hyun Kim[1], G. Khaliullin[2], and B. I. Min[1]
[1] *Department of Physics, PCTP, Pohang University of Science and Technology, Pohang 790-784, Korea*
[2] *Max Planck Institute for Solid State Research, Heisenbergstrasse 1, D-70569 Stuttgart, Germany*
(Dated: February 25, 2014)

We have investigated the excitation spectra of $j_{eff}=\frac{1}{2}$ Mott insulator $Na_2IrO_3$. Taking into account a relativistic multiplet structure of Ir ions, we have calculated the optical conductivity $\sigma(\omega)$ and resonant inelastic x-ray scattering (RIXS) spectra, which manifest different features from those of a canonical $j_{eff}=\frac{1}{2}$ system $Sr_2IrO_4$. Distinctly from the two-peak structure in $Sr_2IrO_4$, $\sigma(\omega)$ in $Na_2IrO_3$ has a broad single peak dominated by interband transitions from $j_{eff}=\frac{3}{2}$ to $\frac{1}{2}$. RIXS spectra exhibit the spin-orbit (SO) exciton that has a two-peak structure arising from the crystal-field effect, and the magnon peak at energies much lower than in $Sr_2IrO_4$. In addition, a small peak near the optical absorption edge is found in RIXS spectra, originating from the coupling between the electron-hole ($e$-$h$) excitation and the SO exciton. Our findings corroborate the validity of the relativistic electronic structure and importance of both itinerant and local features in $Na_2IrO_3$.

PACS numbers: 71.10.Li,71.70.Ej,78.20.Bh

Rich physical properties in $4d$ and $5d$ transition metal (TM) oxides arise from the mutual interplay of electronic degrees of freedom such as bandwidth $W$, Coulomb correlation $U$, and spin-orbit (SO) coupling $\lambda$ [1]. $Sr_2IrO_4$ is one of the most-studied $5d$ TM systems to examine cooperative effects of the electronic degrees of freedom, which yield the intriguing $j_{eff}=\frac{1}{2}$ Mott insulating nature [2–6]. Another iridate $Na_2IrO_3$ also draws the recent attention because of its insulating nature similar to that of $Sr_2IrO_4$. In contrast to $Sr_2IrO_4$ with corner-shared $IrO_6$ octahedra, $Na_2IrO_3$ is composed of edge-shared octahedra (see Fig. 1), and Ir ions form a honeycomb lattice. Early proposals that $Na_2IrO_3$ may be a topological insulator [7] or host Kitaev model physics [4] triggered a theoretical and experimental activity aimed to understand insulating nature and magnetic structure of $Na_2IrO_3$ [8–18].

The strong SO coupling in iridates causes $t_{2g}$ orbitals to split into $j_{eff}=\frac{1}{2}$ and $\frac{3}{2}$ states [see Fig. 1(c)], and then the resulting narrow half-filled $j_{eff}=\frac{1}{2}$ band is to be split even by a weak Coulomb repulsion to become a Mott insulator [2]. This scenario, however, has been questioned recently by Mazin *et al.*[18–20], who argued that the insulating nature of $Na_2IrO_3$ originates from the formation of quasi-molecular orbital (QMO) states of Ir hexagon, which have a considerable itinerant character. Physically, this kind of controversy is evoked due to dual (atomic/band) nature of Ir $5d$ orbitals. Because three relevant physical parameters $W$, $\lambda$, and $U$ of Ir $5d$ orbitals are of similar energy scale, it is not easy to identify which parameter is dominant in determining the electronic structures of iridates.

In fact, dual nature of $5d$ orbitals is reflected on excitations, which manifest various peculiar features in iridates. In the case of $Sr_2IrO_4$, the local $d$-$d$ transition between $j_{eff}=\frac{1}{2}$ and $\frac{3}{2}$, termed as the SO exciton, is observed in resonant inelastic x-ray scattering (RIXS) spectra [5], and optical conductivity $\sigma(\omega)$ exhibits a prominent two-peak structure at 0.5 and 1.0 eV in the vicinity of Mott gap region [21]. $\sigma(\omega)$ and RIXS spectra for $Na_2IrO_3$ display some features distinct from those in $Sr_2IrO_4$. Instead of a two-peak structure, $\sigma(\omega)$ of $Na_2IrO_3$ shows just a broad single peak at higher energy of $\sim 1.5$ eV [17, 22]. SO exciton peak is present in RIXS spectra of $Na_2IrO_3$ too, but it has a well resolved two-peak structure and a negligible momentum dependence. The origin of these two RIXS-peaks is under debate, whether they come from the trigonal crystal-field [23] or not [20]. In addition, an extra RIXS-peak was detected in $Na_2IrO_3$ near the optical absorption edge ($\sim 0.4$ eV), whose origin is not yet settled. It is important to examine the similarities and differences between $Sr_2IrO_4$ and $Na_2IrO_3$ including both correlation and itineracy effects, in order to clarify what kind of electronic nature prevails in these compounds: atomic, band, or dual nature.

In this Letter, we have investigated characteristic features of excitation spectra in $Na_2IrO_3$. More specifically,

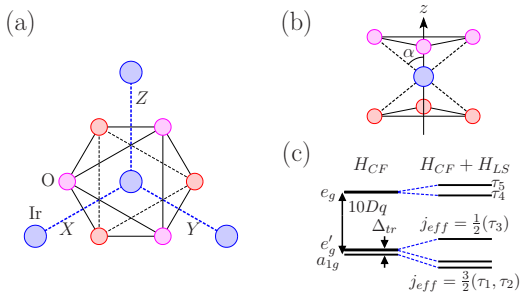


FIG. 1: (Color online) (a) Top view of edge-shared $Na_2IrO_3$. $X$, $Y$, and $Z$ represent directions of nearest neighboring Ir sites. (b) The trigonally compressed $IrO_6$ octahedron, where the angle $\alpha$ between $z$-axis and Ir-O bond direction is about $57.96°$, instead of $\cos^{-1}\sqrt{\frac{1}{3}} \approx 54.74°$ for $O_h$ symmetry. (c) Energy splitting of local $d$ levels in the presence of the trigonal distortion and SO coupling.

we addressed the following questions currently in dispute: (i) why $\sigma(\omega)$ has a single-peak structure distinctly from that of $Sr_2IrO_4$, (ii) what is the origin of two peaks of the SO exciton in RIXS spectra, and (iii) what is the identity of an extra RIXS peak observed near the optical edge. For this purpose, we have generated the microscopic model incorporating the full local multiplets of Ir ions and their hopping integrals. Using the exact diagonalization (ED) method, we have calculated $\sigma(\omega)$ and RIXS spectra for $Na_2IrO_3$, and extracted the physical parameters that best describe the experimental data. We have demonstrated that the coupling between the itinerant $e$-$h$ excitations and the local SO exciton is essential in $Na_2IrO_3$ but, due to different hopping topology in a honeycomb lattice, the manifestations of this effect in $\sigma(\omega)$ and RIXS spectra are different from those in $Sr_2IrO_4$.

To investigate electronic structures of two dimensional honeycomb lattice $Na_2IrO_3$, we considered a four-site Ir cluster as shown in Fig. 1(a). The local Hamiltonian of a Ir site reads as:

$$H_{ion} = \sum_{\mu\sigma} \epsilon_\mu n_{\mu\sigma} + \lambda \sum_{\mu\nu\sigma\sigma'} (\mathbf{l}\cdot\mathbf{s})_{\mu\sigma,\nu\sigma'} c^\dagger_{\mu\sigma} c_{\nu\sigma'} + \frac{1}{2}\sum_{\sigma\sigma'\mu\nu} U_{\mu\nu} c^\dagger_{\mu\sigma} c^\dagger_{\nu\sigma'} c_{\nu\sigma'} c_{\mu\sigma} + \frac{1}{2}\sum_{\substack{\sigma\sigma'\\ \mu\neq\nu}} J_{\mu\nu} c^\dagger_{\mu\sigma} c^\dagger_{\nu\sigma'} c_{\mu\sigma'} c_{\nu\sigma} + \frac{1}{2}\sum_{\substack{\sigma\\ \mu\neq\nu}} J'_{\mu\nu} c^\dagger_{\mu\sigma} c^\dagger_{\mu-\sigma} c_{\nu-\sigma} c_{\nu\sigma}, \quad (1)$$

where $\mu$ and $\sigma$ refer to orbital and spin states of Ir, respectively. Because of the trigonal distortion [24] and the strong SO coupling (first and second terms in Eq. 1), Ir $5d$ orbitals are split into five double group states ($\tau_1$-$\tau_5$), as shown in Fig. 1(c) [25]. $U_{\mu\nu}$ , $J_{\mu\nu}$ , and $J'_{\mu\nu}$ are direct Coulomb, exchange Coulomb, and pair hopping integrals, which can be given by $U$ and $J_H$ parameters [26]. Figure 2(a) presents local electronic energies of Ir multiplets calculated with physical parameters in Table I. Because $10Dq$ is large enough ($\sim$ 3.3 eV), the lowest three double group states ($\tau_1$,$\tau_2$,$\tau_3$) mainly contribute to low energy multiplets of $d^4$, $d^5$, and $d^6$ configurations, see Fig. 2(b). In describing the Hilbert space of the four-site cluster, we took into account several lowest multiplets, *e.g.*, six ($\bar{D}$,$\bar{Q}$) for $d^5$, fourteen ($\bar{S}$,$\bar{T}$,$\bar{P}$,$\bar{P}'$) for $d^4$, and one ($\bar{A}$) for $d^6$. Note that $\bar{S}$ corresponds to the hole state mainly of $j_{eff}$=$\frac{1}{2}$ band, whereas $\bar{T}$, $\bar{P}$, and $\bar{P}'$ correspond to those of $j_{eff}$=$\frac{3}{2}$ bands.

TABLE I: Physical parameters of $Na_2IrO_3$ in units of eV. They are adopted to be consistent with literature ($\Delta$ [17], $\Delta_{tr}$ [20]) and to optimize theoretical RIXS spectra ($10Dq$, $J_H$, $\lambda$, $t_{pd\sigma}$) and $\sigma(\omega)$ ($U$).

| $10Dq$ | $\Delta$ | $\Delta_{tr}$ | $U$ | $J_H$ | $\lambda$ | $t_{pd\sigma}$ | $t_{pd\pi}$ |
|---|---|---|---|---|---|---|---|
| 3.3 | 3.3 | 0.075 | 1.35 | 0.25 | 0.43 | $-1.90$ | $-0.46t_{pd\sigma}$ |

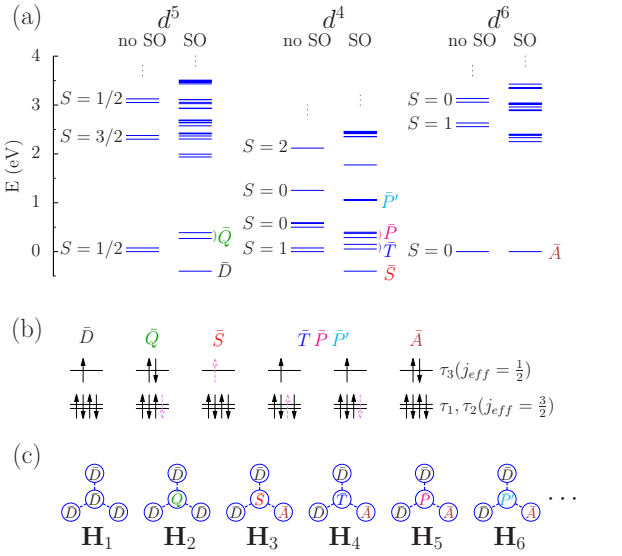


FIG. 2: (Color online) (a) Relative energies for $d^4$, $d^5$, and $d^6$ multiplets of $Na_2IrO_3$ with physical parameters from Table I. When the trigonal distortion is absent ($\Delta_{tr}$=0.0), each $\bar{Q}$, $\bar{T}$, $\bar{P}$, and $\bar{P}'$ multiplets are degenerate. (b) Relevant configurations that give dominant contributions to low energy multiplets. Violet dotted arrows represent removed spins from $\bar{D}$ multiplet. Because $10Dq$ is large enough, isospins in relevant multiplets occupy three double group levels ($\tau_1, \tau_2, \tau_3$), which are mainly attributed to $t_{2g}$ manifolds ($j_{eff}$=$\frac{1}{2}$, $j_{eff}$=$\frac{3}{2}$). But we consider all the five double group states ($\tau_1$-$\tau_5$) in describing the multiplets. (c) Schematic diagrams of possible cluster multiplets included in each subspace.

In order to save computational cost, we restricted the Hilbert space into all possible multiplets of $d^5$-$d^5$-$d^5$-$d^5$ and $d^4$-$d^6$-$d^5$-$d^5$ configurations, which are expressed as the direct product of relevant multiplets of Ir ions ($\bar{D}\cdots\bar{A}$). Because this restricted space already includes all possible states with energies lower than 2.0 eV, it will provide appropriate details of low energy excitations in $Na_2IrO_3$. To discern excitation distributions, we classified the Hilbert space into seven subspaces: $\mathbf{H}_1$-$\mathbf{H}_7$ [27]. Some examples included in each subspace are shown in Fig. 2(c). To include the itineracy effects, we considered the hopping between nearest neighboring (NN) Ir's via intermediate oxygen [28]. Employing the Slater-Koster theory [29], we calculated the $pd$-hopping matrix in terms of $t_{pd\sigma}$ and $t_{pd\pi}$ parameters and evaluated the effective hopping $t_{dd}(\tau\tilde{\sigma};\tau'\tilde{\sigma}')$ between NN double group states $\tau\tilde{\sigma}$ and $\tau'\tilde{\sigma}'$ by summing $\sum_{p\sigma} \frac{t_{pd}(\tau\tilde{\sigma};p\sigma)t^*_{pd}(\tau'\tilde{\sigma}';p\sigma)}{\sqrt{(\Delta+\epsilon_\tau)(\Delta+\epsilon_{\tau'})}}$ values of two Ir-O-Ir paths ($\Delta$ is $p$-$d$ charge transfer energy) [30].

Using the ED method, we have solved the Hamiltonian of the four-site cluster and investigated the excitation spectra. Let $E_n$ and $|\Psi_n\rangle$ be the $n$-th eigenvalue and the eigenvector of the cluster, respectively. To examine the excitation distribution, we obtained

the projected excitation spectrum (PES) as $\Lambda_i(\omega) = \sum_n \sum_{m\in\mathbf{H}_i} |\langle\Psi_n|m\rangle|^2\delta(\omega - E_n)$, where $|m\rangle$ represents the orthonormal basis of the subspace $\mathbf{H}_i$. To compare theoretical PES to observed excitations in $Na_2IrO_3$, we calculated $\sigma(\omega)$ and RIXS spectra by using the Kubo formula [6]. We set $k_BT = 30$ meV.

Figure 3(a) shows the PES for $Na_2IrO_3$. Let us first explore the relation between a specific PES and each excitation. Because $\mathbf{H}_1$ includes all possible fluctuations of isospin $J_{eff}$=1/2 for $d^5$, $\Lambda_1$ ($\bar{D}\bar{D}\bar{D}\bar{D}$) represents the magnon excitation. $\Lambda_2$ ($\bar{D}\bar{Q}\bar{D}\bar{D}$) represents one or more SO excitons because $\bar{Q}$ is one hole state of $j_{eff}$=$\frac{3}{2}$ for $d^5$ [Fig. 2(b)]. $\Lambda_3$ ($\bar{A}\bar{S}\bar{D}\bar{D}$) and $\Lambda_4$-$\Lambda_6$ are related to the $e$-$h$ excitations involving hole states of $j_{eff}$=$\frac{1}{2}$ ($\bar{S}$) and $j_{eff}$=$\frac{3}{2}$ ($\bar{T}$, $\bar{P}$, $\bar{P}'$), respectively.

We can notice interesting features in the PES of Fig. 3. (1) $\Lambda_1$ shows a magnon peak at low energies, below 50 meV. This feature is very different from that of $Sr_2IrO_4$, in which magnon spectra spread over 0-250 meV [6]. It implies strong suppression of the magnetic interaction in $Na_2IrO_3$ due to its edge-shared bonding nature. Because the Ir-O-Ir bond angle is nearly 90°, the effective hopping between $j_{eff}$=$\frac{1}{2}$ ($\tau_3$) states is suppressed a lot. Actually, this hopping is almost one-order of magnitude smaller than that between $j_{eff}$=$\frac{1}{2}$ and $\frac{3}{2}$ ($\tau_1$) states [30]. (2) $\Lambda_2$ exhibits two peaks at 0.73 and 0.86 eV. This spectrum is attributed to the on-site $d$-$d$ transition from occupied $j_{eff}$=$\frac{3}{2}$ ($\tau_1$,$\tau_2$) to unoccupied $j_{eff}$=$\frac{1}{2}$ ($\tau_3$), which is reminiscent of the SO exciton in $Sr_2IrO_4$. Indeed, as will be shown in Fig. 4(a), this spectrum is consistent with experimental RIXS peak positions for $Na_2IrO_3$ [23]. $\Lambda_2$ has peaks above 1.0 eV too. They, however, hardly produce RIXS spectra because they correspond to two or more simultaneous SO excitons. (3) $\Lambda_3$ spreads over broad energy range above $\omega \approx 0.4$ eV. It does not look like a single peak corresponding to the $\bar{A}\bar{S}\bar{D}\bar{D}$ multiplet, which indicates that simple atomic picture is inadequate to describe the $j_{eff}$=$\frac{1}{2}$ $e$-$h$ excitation of $Na_2IrO_3$. There should be considerable mixing among a few multiplets due to itinerant character of Ir 5$d$ bands. Moreover, $\Lambda_3$ shows a small peak near the $e$-$h$ excitation edge ($\omega \sim 0.4$ eV). Interestingly, $\Lambda_2$ also has a peak in the same region with almost the same intensity. This feature suggests that there is a strong mixing between $\Lambda_2$ and $\Lambda_3$, which is supposed to produce both the broad dispersion and the edge state in $\Lambda_3$. (4) $\Lambda_4$-$\Lambda_6$ are distributed above $\omega$ =1.2 eV. Despite their broad dispersions, each PES has its own predominant peak, implying that local multiplets of $j_{eff}$=$\frac{3}{2}$ hole are retained. As shown in Fig. 3(b), in this region of $\sim$ 1.5 eV, there appears a broad peak of $\sigma(\omega)$ in $Na_2IrO_3$. It is thus expected that the interband $e$-$h$ transitions from $j_{eff}$=$\frac{3}{2}$ to $\frac{1}{2}$ ($\bar{T}$,$\bar{P}$,$\bar{P}'$) give rise to main spectral weight in $\sigma(\omega)$ of $Na_2IrO_3$.

Figure 3(b) presents theoretical result for $\sigma(\omega)$. Similar to experimental data, it exhibits a predominant peak at around 1.5 eV, which certainly reflects the major

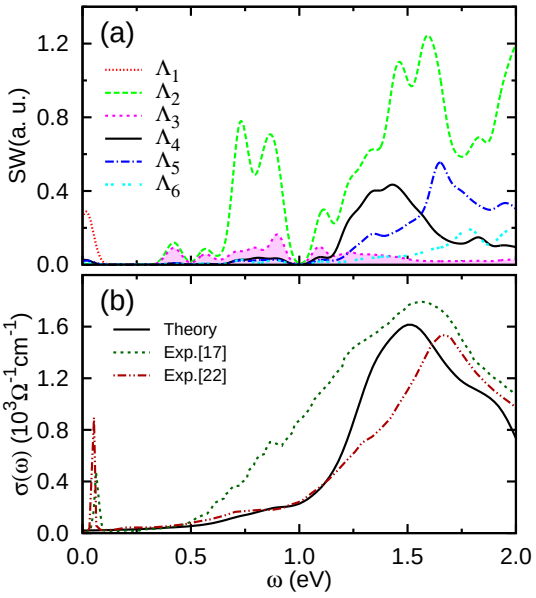


FIG. 3: (Color online) (a) Spectral weight (SW) of projected excitation spectra (PES) for $Na_2IrO_3$. (b) Optical conductivity of $Na_2IrO_3$ as calculated (solid line) and measured at $T$ = 300 K (dotted line [17], dot-dashed line [22]). The observed sharp peak near 0.1 eV is of phonon origin (not included in our calculations).

role of $j_{eff}$=$\frac{3}{2}$ states, as explained above. The spectral weight of $j_{eff}$=$\frac{1}{2}$ band (which dominates in $Sr_2IrO_4$) is suppressed because of hopping topology of edge-shared $Na_2IrO_3$. This behavior in $Na_2IrO_3$ is contrary to that in $Sr_2IrO_4$, for which two prominent peaks of $j_{eff}$=$\frac{1}{2}$ band origin appear through the Fano-type overlap between the $e$-$h$ continuum of the $j_{eff}$=$\frac{1}{2}$ band and the on-site SO exciton [6].

Shown in Figure 4(a) is the theoretical RIXS spectra at $\mathbf{q} = 0$ [31]. Noteworthy is the emergence of three-peak structure (denoted by $A$, $B$, and $C$), which is consistent with the experiment. To elucidate the origin of these three peaks, we also calculated RIXS spectra for a single-site $IrO_6$ cluster, including all possible $d^5$ multiplets. In this case, only two peaks appear at 0.67 and 0.78 eV [see inset of Fig. 4(a)], which are equivalent to $B$ and $C$ peaks for the four-site cluster. This implies that both $B$ and $C$ correspond to local excitations, which are attributed to on-site $d$-$d$ transitions between $j_{eff}$ = $\frac{1}{2}$ and $\frac{3}{2}$ orbitals. Then it is natural to conjecture that the energy difference between $B$ and $C$ comes from the crystal-field splitting of $j_{eff}$=$\frac{3}{2}$ states. Indeed, as shown in Fig. 4(b), the splitting between $B$ and $C$ increases with increasing the trigonal distortion strength of $\Delta_{tr}$. We point out that the observed $B$-$C$ splitting of the order of 110 meV is well explained by our calculations which include correlation effects, even though we used a rather small input value of $\Delta_{tr}$ = 75 meV [20]. This can be understood as a correlation-induced enhancement of the crystal-field

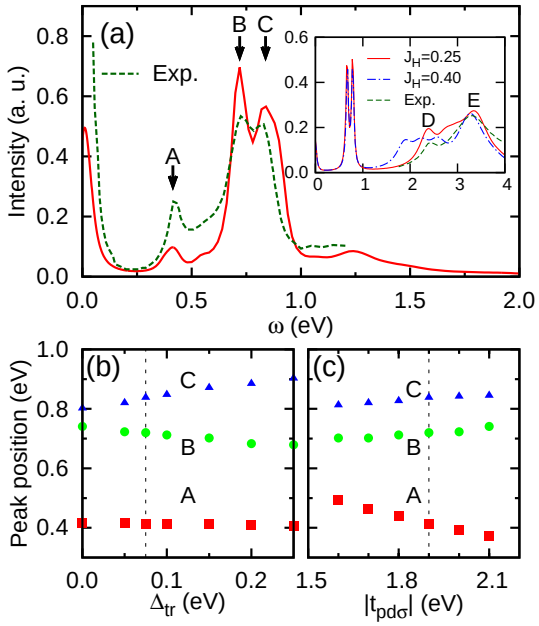


FIG. 4: (Color online) (a) Calculated RIXS spectra (solid line) for the four-site cluster of $Na_2IrO_3$. Dashed line: experimental data measured at room temperature [23]. Inset: calculated RIXS spectra for a single-site cluster incorporating all possible $d^5$ multiplets at two different $J_H$. Peak positions as functions of (b) the trigonal distortion and (c) the hopping strength. Vertical lines in (b) and (c) denote the possible optimal parameters of $\Delta_{tr}$ and $t_{pd\sigma}$.

splitting [32].

It is seen in Fig. 4(a) that the peak $A$ near 0.4 eV is missing in the single-site calculation of inset. This finding suggests that the peak $A$ is related to itinerant nature of Ir $5d$ orbitals, especially, the inter-site hopping between $j_{eff} = \frac{1}{2}$ and $\frac{3}{2}$ states, which is dominant here [30]. We already noticed in the PES of Fig. 3(a) that there is a strong coupling between SO exciton $\Lambda_2$ and $e$-$h$ continuum $\Lambda_3$ in the vicinity of peak $A$. More convincing evidence is found in Fig. 4(c), which presents the peak positions as a function of the hopping strength. We note that the larger the hopping strength is, the lower the peak position of $A$ is. This behavior reveals that the peak $A$ at the edge of $e$-$h$ excitation certainly originates from the inter-site hopping, which brings about the coupling of broad $e$-$h$ continuum with the local SO exciton. Note that, this $e$-$h$ excitation is hardly detectable in the optical spectra. It is due to the large suppression of the direct hopping between $j_{eff} = \frac{1}{2}$ bands in the edge-shared of $Na_2IrO_4$. This finding is different from a suggestion of Ref. 23 that the peak $A$ is an excitonic bound state due to long-range Coulomb interaction.

The single-site calculation in the inset of Fig. 4(a) also gives $D$ and $E$ peaks above 2.0 eV, which are in good agreement with experiment [23]. Note that the peak position of $D$ moves with varying $J_H$, while that of $E$ does not. Both $D$ and $E$ correspond to local excitations to $t_{2g}^4 e_g^1$ configurations. But they have different spin states: $D$ has high-spin $S$=$\frac{3}{2}$ while $E$ has low-spin $S$=$\frac{1}{2}$, as shown in Fig. 2(a) for $d^5$. Energies of the former and the latter with respect to the ground state are given by $10Dq - 4J_H$ and $10Dq$, respectively. Accordingly, from the peak positions of $D$ and $E$, one can determine $10Dq$ and $J_H$ values.

Our RIXS calculation yields the magnetic peak below ∼50 meV, in a qualitative agreement with the recent RIXS experiment for $Na_2IrO_3$, where the magnetic excitations dispersing up to energy of ∼35 meV have been observed [33]. The agreement is not surprising since our calculations fully include the exchange processes discussed in Ref. 16 that contribute to Kitaev-Heisenberg interactions (except a direct hopping between Ir's which is small [18]).

Our successful description of various excitations in $Na_2IrO_3$ indicate the realization of the relativistic electronic structure in this material. According to recent DFT calculation [34], the majority of Wannier orbitals near the Fermi level have indeed a dominant $j_{eff}$=$\frac{1}{2}$ character, with only small $j_{eff}$=$\frac{3}{2}$ tails on the NN sites. More importantly, the results presented above make it clear that both itinerant and local features have to be accounted for to describe the experimental observations.

In conclusion, we have clarified controversial issues of $Na_2IrO_3$, by unraveling the identities of low energy excitations observed in $\sigma(\omega)$ and RIXS spectra. The broad peak of $\sigma(\omega)$ in $Na_2IrO_3$ is attributed to $e$-$h$ excitations from $j_{eff}$=$\frac{3}{2}$ to $\frac{1}{2}$ bands, in contrast to $Sr_2IrO_4$ where two-peak structure arises from $e$-$h$ excitations of $j_{eff}$=$\frac{1}{2}$ band through the Fano-type overlap with the on-site SO exciton. Two peaks at 0.7-0.8 eV in RIXS spectra of $Na_2IrO_3$ come from local $d$-$d$ transitions between two relativistic states, and their splitting is caused by the trigonal crystal-field enhanced by correlation effects. The RIXS peak found in $Na_2IrO_3$ near $\omega \sim 0.4$ eV originates from the coupling between the $e$-$h$ excitation of $j_{eff}$=$\frac{1}{2}$ band and the SO exciton in the vicinity of optical absorption edge. Altogether, our study confirms the relativistic Mott insulating nature of $Na_2IrO_3$, and demonstrates that the Fano-type coupling between the itinerant $e$-$h$ excitations and the local SO transition is an intrinsic nature in iridate systems including both $Na_2IrO_3$ and $Sr_2IrO_4$.

We thank B. J. Kim and Heung-Sik Kim for fruitful discussions. This work was supported by the NRF (No.2009-0079947).

[1] D. Pesin and L. Balents, Nature Phys. **6**, 376 (2010)
[2] B.J. Kim, H. Jin, S.J. Moon, J.-Y. Kim, B.-G. Park, C.S. Leem, J. Yu, T.W. Noh, C. Kim, S.-J. Oh, J.-H. Park, V. Durairaj, G. Cao, and E. Rotenberg, Phys. Rev. Lett.

**101**, 076402 (2008).
[3] B.J. Kim, H. Ohsumi, T. Komesu, S. Sakai, T. Morita, H. Takagi, and T. Arima, Science **323**, 1329 (2009).
[4] G. Jackeli and G. Khaliullin, Phys. Rev. Lett. **102**, 017205 (2009).
[5] J. Kim, D. Casa, M.H. Upton, T. Gog, Y.-J. Kim, J.F. Mitchell, M. van Veenendaal, M. Daghofer, J. van den Brink, G. Khaliullin, and B.J. Kim, Phys. Rev. Lett. **108**, 177003 (2012).
[6] B.H. Kim, G. Khaliullin, and B.I. Min, Phys. Rev. Lett. **109**, 167205 (2012).
[7] A. Shitade, H. Katsura, J. Kuneѕ, X.-L. Qi, S.-C. Zhang, and N. Nagaosa, Phys. Rev. Lett. **102**, 256403 (2009).
[8] H. Jin, H. Kim, H. Jeong, C.H. Kim, and J. Yu, arXiv:0907.0743; C.H. Kim, H.S. Kim, H. Jeong, H. Jin, and J. Yu, Phys. Rev. Lett. **108**, 106401 (2012).
[9] Y. Singh and P. Gegenwart, Phys. Rev. B **82**, 064412 (2010).
[10] J. Chaloupka, G. Jackeli, and G. Khaliullin, Phys. Rev. Lett. **105**, 027204 (2010).
[11] X. Liu, T. Berlijn, W.-G. Yin, W. Ku, A. Tsvelik, Y.-J. Kim, H. Gretarsson, Y. Singh, P. Gegenwart, and J.P. Hill, Phys. Rev. B **83**, 220403(R) (2011).
[12] Y. Singh, S. Manni, J. Reuther, T. Berlijn, R. Thomale, W. Ku, S. Trebst, and P. Gegenwart, Phys. Rev. Lett. **108**, 127203 (2012).
[13] S.K. Choi, R. Coldea, A.N. Kolmogorov, T. Lancaster, I.I. Mazin, S.J. Blundell, P.G. Radaelli, Y. Singh, P. Gegenwart, K.R. Choi, S.-W. Cheong, P.J. Baker, C. Stock, and J. Taylor, Phys. Rev. Lett. **108**, 127204 (2012).
[14] F. Ye, S. Chi, H. Cao, B.C. Chakoumakos, J.A. Fernandez-Baca, R. Custelcean, T.F. Qi, O.B. Korneta, and G. Cao, Phys. Rev. B **85**, 180403(R) (2012).
[15] I. Kimchi and Y.Z. You, Phys. Rev. B **84**, 180407(R) (2011).
[16] J. Chaloupka, G. Jackeli, and G. Khaliullin, Phys. Rev. Lett. **110**, 097204 (2013).
[17] R. Comin, G. Levy, B. Ludbrook, Z.-H. Zhu, C.N. Veenstra, J.A. Rosen, Y. Singh, P. Gegenwart, D. Stricker, J.N. Hancock, D. van der Marel, I.S. Elfimov, and A. Damascelli, Phys. Rev. Lett. **109**, 266406 (2012).
[18] I.I. Mazin, H.O. Jeschke, K. Foyevtsova, R. Valenti, and D.I. Khomskii, Phys. Rev. Lett. **109**, 197201 (2012).
[19] I.I. Mazin, S. Manni, K. Foyevtsova, H.O. Jeschke, P. Gegenwart, and R. Valenti, Phys. Rev. B **88**, 035115 (2013).
[20] K. Foyevtsova, H.O. Jeschke, I.I Mazin, D.I. Khomskii, and R. Valenti, Phys. Rev. B **88**, 035107 (2013).
[21] S.J. Moon, H. Jin, W.S. Choi, J.S. Lee, S.S.A. Seo, J. Yu, G. Cao, T.W. Noh, and Y.S. Lee, Phys. Rev. B **80**, 195110 (2009).
[22] C.H. Sohn, H.-S. Kim, T.F. Qi, D.W. Jeong, H.J. Park, H.K. Yoo, H.H. Kim, J.-Y. Kim, T.D. Kang, D.-Y. Cho, G. Cao, J. Yu, S.J. Moon, and T.W. Noh, Phys. Rev. B **88**, 085125 (2013).
[23] H. Gretarsson, J.P. Clancy, X. Liu, J.P. Hill, E. Bozin, Y. Singh, S. Manni, P. Gegenwart, J. Kim, A.H. Said, D. Casa, T. Gog, M.H. Upton, H.-S. Kim, J. Yu, V.M. Katukuri, L. Hozoi, J. van den Brink, and Y.-J. Kim, Phys. Rev. Lett **110**, 076402 (2013).
[24] A monoclinic $Na_2IrO_3$ ($C2/m$ space group) suffers from several structural deformations such as orthorhombic distortion, octahedra rotations, and trigonal distortion [13]; the latter has the most impact on the electronic structure [20].
[25] See Supplemental Material for relativistic orbital shapes of double group states.
[26] $U_{\mu\mu} = U$, $U_{\mu\neq\nu} = U - 2J_H$, and $J_{\mu\nu} = J'_{\mu\nu} = J_H$.
[27] The Hilbert space is classified into seven subspaces: $\mathbf{H}_1$ of four $\bar{D}$'s of $d^5$, $\mathbf{H}_2$ of one or more $\bar{Q}$ among four $d^5$ configurations, $\mathbf{H}_3$ of two $\bar{D}$'s of $d^5$ and an $\bar{A}$-$\bar{S}$ $e$-$h$ pair, $\mathbf{H}_4$ of two $\bar{D}$'s of $d^5$ and an $\bar{A}$-$\bar{T}$ $e$-$h$ pair, $\mathbf{H}_5$ of two $\bar{D}$'s of $d^5$ and an $\bar{A}$-$\bar{P}$ $e$-$h$ pair , $\mathbf{H}_6$ of two $\bar{D}$'s of $d^5$ and an $\bar{A}$-$\bar{P}'$ $e$-$h$ pair, and others ($\mathbf{H}_7$).
[28] In our calculation, the next or third NN hopping and the direct Ir-Ir hopping are not included, because the strength of the NN hopping mediated by oxygen is much larger than other hoppings [18].
[29] J.C. Slater and G.F. Koster, Phys. Rev. **94**, 1498 (1954).
[30] See Supplemental Material for hopping strengths between neighboring double group states.
[31] To calculate the RIXS spectra, we assumed that both incident and outgoing angles of x-ray are 45°, and the incident and outgoing beams have $\sigma$ and arbitrary polarizations, respectively.
[32] A.I. Poteryaev, J.M. Tomczak, S. Biermann, A. Georges, A.I. Lichtenstein, A.N. Rubtsov, T. Saha-Dasgupta, and O.K. Andersen, Phys. Rev. B **76**, 085127 (2007).
[33] H. Gretarsson, J.P. Clancy, Y. Singh, P. Gegenwart, J.P. Hill, J. Kim, M.H. Upton, A.H. Said, D. Casa, T. Gog, Y.-J. Kim, Phys. Rev. B **87**, 220407(R) (2013).
[34] H.-S. Kim, C.H. Kim, H. Jeong, H. Jin, and J. Yu, Phys. Rev. B **87**, 165117 (2013).

*Supplemental Material:*

# Electronic excitations in the edge-shared relativistic Mott insulator: $Na_2IrO_3$

## RELATIVISTIC ORBITAL STATES

In the trigonal distortion (see Fig. 1(b)), $d$ orbital states are split into the following eigenstates:

$$
\begin{aligned}
|e'_{g1}\rangle &= \cos\alpha'|xy\rangle - \sin\alpha'|yz\rangle,\\
|e'_{g2}\rangle &= \cos\alpha'|x^2-y^2\rangle + \sin\alpha'|zx\rangle,\\
|a_{1g}\rangle &= |z^2\rangle,\\
|e_{g1}\rangle &= \cos\alpha'|zx\rangle - \sin\alpha'|x^2-y^2\rangle,\\
|e_{g2}\rangle &= \cos\alpha'|yz\rangle + \sin\alpha'|xy\rangle.
\end{aligned}
$$

Note that, when $\cos\alpha' = \sqrt{\frac{2}{3}} \approx 0.816$, $e'_g$ and $a_{1g}$ orbitals correspond to $t_{2g}$ orbitals in the local $O_h$ symmetry. In the presence of the trigonal distortion, $\cos\alpha'$ is to be reduced from $\sqrt{\frac{2}{3}}$. In our calculation for $Na_2IrO_3$, we have adopted $\cos\alpha' \approx 0.776$ to fit $10Dq$ and $\Delta_{tr}$ parameters based on the crystal field calculation[S1]. Thus, the double group states for given parameters in Table I are expressed as following:

$$
\begin{aligned}
|\tau_1\tilde{\uparrow}\rangle &\approx 0.811|a_{1g}\uparrow\rangle - 0.402i\left(|e'_{g1}\downarrow\rangle + i|e'_{g2}\downarrow\rangle\right) + 0.098\left(|e_{g1}\downarrow\rangle + i|e_{g2}\downarrow\rangle\right),\\
|\tau_2\tilde{\uparrow}\rangle &\approx 0.437\left(|e'_{g1}\uparrow\rangle + i|e'_{g2}\uparrow\rangle\right) + 0.028i\left(|e_{g1}\uparrow\rangle + i|e_{g2}\uparrow\rangle\right) - 0.545\left(|e'_{g1}\downarrow\rangle - i|e'_{g2}\downarrow\rangle\right) - 0.103i\left(|e_{g1}\downarrow\rangle - i|e_{g2}\downarrow\rangle\right),\\
|\tau_3\tilde{\uparrow}\rangle &\approx 0.579\left(|e'_{g1}\uparrow\rangle - i|e'_{g2}\uparrow\rangle\right) - 0.006i\left(|e_{g1}\uparrow\rangle - i|e_{g2}\uparrow\rangle\right) - 0.575i|a_{1g}\downarrow\rangle,\\
|\tau_4\tilde{\uparrow}\rangle &\approx -0.077\left(|e'_{g1}\uparrow\rangle + i|e'_{g2}\uparrow\rangle\right) - 0.690i\left(|e_{g1}\uparrow\rangle + i|e_{g2}\uparrow\rangle\right) - 0.075\left(|e'_{g1}\downarrow\rangle - i|e'_{g2}\downarrow\rangle\right) - 0.115i\left(|e_{g1}\downarrow\rangle - i|e_{g2}\downarrow\rangle\right),\\
|\tau_5\tilde{\uparrow}\rangle &\approx 0.061\left(|e'_{g1}\uparrow\rangle - i|e'_{g2}\uparrow\rangle\right) + 0.700i\left(|e_{g1}\uparrow\rangle - i|e_{g2}\uparrow\rangle\right) + 0.109i|a_{1g}\downarrow\rangle,\\
|\tau_1\tilde{\downarrow}\rangle &\approx 0.402\left(|e'_{g1}\uparrow\rangle - i|e'_{g2}\uparrow\rangle\right) - 0.098i\left(|e_{g1}\uparrow\rangle - i|e_{g2}\uparrow\rangle\right) + 0.811i|a_{1g}\downarrow\rangle,\\
|\tau_2\tilde{\downarrow}\rangle &\approx 0.545\left(|e'_{g1}\uparrow\rangle + i|e'_{g2}\uparrow\rangle\right) - 0.103i\left(|e_{g1}\uparrow\rangle + i|e_{g2}\uparrow\rangle\right) + 0.437\left(|e'_{g1}\downarrow\rangle - i|e'_{g2}\downarrow\rangle\right) - 0.028i\left(|e_{g1}\downarrow\rangle - i|e_{g2}\downarrow\rangle\right),\\
|\tau_3\tilde{\downarrow}\rangle &\approx 0.575|a_{1g}\uparrow\rangle + 0.579i\left(|e'_{g1}\downarrow\rangle + i|e'_{g2}\downarrow\rangle\right) - 0.006\left(|e_{g1}\downarrow\rangle + i|e_{g2}\downarrow\rangle\right),\\
|\tau_4\tilde{\downarrow}\rangle &\approx 0.075\left(|e'_{g1}\uparrow\rangle + i|e'_{g2}\uparrow\rangle\right) - 0.115i\left(|e_{g1}\uparrow\rangle + i|e_{g2}\uparrow\rangle\right) - 0.077\left(|e'_{g1}\downarrow\rangle - i|e'_{g2}\downarrow\rangle\right) + 0.690i\left(|e_{g1}\downarrow\rangle - i|e_{g2}\downarrow\rangle\right),\\
|\tau_5\tilde{\downarrow}\rangle &\approx 0.109|a_{1g}\uparrow\rangle - 0.061i\left(|e'_{g1}\downarrow\rangle + i|e'_{g2}\downarrow\rangle\right) - 0.700\left(|e_{g1}\downarrow\rangle + i|e_{g2}\downarrow\rangle\right).
\end{aligned}
$$

Due to the time-reversal symmetry, all double group pairs are satisfied with $\mathcal{T}|\tau_a\tilde{\uparrow}\rangle = e^{i\delta_a}|\tau_a\tilde{\downarrow}\rangle$, where $\mathcal{T}$ is the time-reversal operator and $\delta_a$ is the phase term raised by numerical process. However, $\delta_a$ does not cause any calculation complexity.

## HOPPING HAMILTONIAN

To describe the hopping interaction, we adopted the tight binding method based on the linear combination of atomic obritals (LCAO). Because the double group state $\tau$ with $\tilde{\sigma}$ isospin is expressed by $|\tau\tilde{\sigma}\rangle = \sum_{\mu\sigma} U_{\tau\tilde{\sigma},\mu\sigma}|\mu\sigma\rangle$, where $U_{\tau\tilde{\sigma},\mu\sigma}$ is the unitary transformation between $\tau\tilde{\sigma}$ and conventional $d$ orbital and spin, the $pd$-hopping matrix is written by $t_{pd}(\tau\tilde{\sigma};p\sigma) = \sum_{\mu\sigma'} U_{\tau\tilde{\sigma},\mu\sigma'}\delta_{\sigma\sigma'}\langle p|V_h|\mu\rangle$, where $\langle p|V_h|\mu\rangle$ is the hopping strength between $p$ and $d$ atomic orbitals. $\langle p|V_h|\mu\rangle$ is a function of two parameters ($t_{pd\sigma}$ and $t_{pd\pi}$) and normal displacement vector between Ir and O. Next, we estimated the effective hopping between nearest neighboring (NN) Ir's based on the second-order perturbation because the charge transfer energy ($\Delta$) is much larger than the $pd$-hopping strengths. In this limit, $t_{dd}(\tau\tilde{\sigma};\tau'\tilde{\sigma}')$ between NN double group states $\tau\tilde{\sigma}$ and $\tau'\tilde{\sigma}'$ is calculated by summing $\sum_{p\sigma}\frac{t_{pd}(\tau\tilde{\sigma};p\sigma)t^*_{pd}(\tau'\tilde{\sigma}';p\sigma)}{\sqrt{(\Delta+\epsilon_\tau)(\Delta+\epsilon_{\tau'})}}$ for two different Ir-O-Ir paths. The hopping Hamiltonian between $i$ and $j$-th Ir's is as following:

$$
H_{ij} = \sum_{\tau_i\tilde{\sigma}_i\tau'_j\tilde{\sigma}'_j} t_{dd}(\tau_i\tilde{\sigma}_i;\tau'_j\tilde{\sigma}'_j)c^\dagger_{\tau'_j\tilde{\sigma}'_j}c_{\tau_i\tilde{\sigma}_i} + h.c.. \tag{2}
$$

Note that the full hopping matrix $(10\times10)$ is Hermitian. Namely, the full hopping matrix elements satisfy the relation such that $\langle\tau_a\tilde{\downarrow}|H_t|\tau_b\tilde{\uparrow}\rangle = \overline{\langle\tau_b\tilde{\uparrow}|H_t|\tau_a\tilde{\downarrow}\rangle}$. Table S1 and S2 present the hopping matrix between neighboring Ir's along the $y$-axis. The hopping between $\tau_1\tilde{\downarrow}$ and $\tau_3\tilde{\uparrow}$ (0.2074) is strongest one, which is about ten times larger than that between $\tau_3\tilde{\uparrow}$'s (0.0219).

TABLE S1: Hopping parameters between neighboring double group state with same isospins in units of eV.

| | $\tau_1\tilde{\uparrow}$ | $\tau_2\tilde{\uparrow}$ | $\tau_3\tilde{\uparrow}$ | $\tau_4\tilde{\uparrow}$ | $\tau_5\tilde{\uparrow}$ |
|---|---|---|---|---|---|
| $\tau_1\tilde{\uparrow}$ | 0.1362 | 0.0797$i$ | 0.0213$i$ | 0.1348$i$ | -0.1125$i$ |
| $\tau_2\tilde{\uparrow}$ | -0.0797$i$ | -0.0520 | -0.0975 | 0.1306 | -0.1186 |
| $\tau_3\tilde{\uparrow}$ | -0.0213$i$ | -0.0975 | 0.0219 | -0.1301 | 0.1119 |
| $\tau_4\tilde{\uparrow}$ | -0.1348$i$ | 0.1306 | -0.1301 | 0.0558 | 0.0709 |
| $\tau_5\tilde{\uparrow}$ | 0.1125$i$ | -0.1186 | 0.1119 | 0.0709 | 0.0976 |

TABLE S2: Hopping parameters between neighboring double group state with different isospins in units of eV.

| | $\tau_1\tilde{\uparrow}$ | $\tau_2\tilde{\uparrow}$ | $\tau_3\tilde{\uparrow}$ | $\tau_4\tilde{\uparrow}$ | $\tau_5\tilde{\uparrow}$ |
|---|---|---|---|---|---|
| $\tau_1\tilde{\downarrow}$ | 0.0000 | -0.0212 | -0.2074 | -0.0933 | 0.0978 |
| $\tau_2\tilde{\downarrow}$ | 0.0212$i$ | 0.0000 | -0.1504 | 0.1426 | -0.1322 |
| $\tau_3\tilde{\downarrow}$ | 0.2074 | -0.1504$i$ | 0.0000 | 0.0362$i$ | -0.0679$i$ |
| $\tau_4\tilde{\downarrow}$ | 0.0933$i$ | -0.1426 | 0.0362 | 0.0000 | -0.0130 |
| $\tau_5\tilde{\downarrow}$ | 0.0978 | 0.1322$i$ | -0.0679$i$ | 0.0130$i$ | 0.0000 |

[S1] K. Yosida, *Theory of magnetism*, (Springer, New York, 1996).